

Project title

Numerical and experimental study of the lateral
impact on composite components

Report on the period of
01/01/2021 to 01/06/2021

By Pouria Bahrami Ataabadi

Supervisor: Prof. Dr. Marcilio Alves

Abstract

This report is divided into three parts; Part I covers the preparation of the VUMAT subroutine for studying the crushing of composite components by using ABAQUS, the second part will cover experimental activities that have been done at the GMSIE laboratory yet and the third part covers the other activities.

Part I: User-defined material VUMAT subroutine and first publication (PP:2-32).

Part II: Experimental and other activities at GMSIE laboratory (PP:33-40).


Part III: Other activities (PP: 41)

Part I: User-defined material VUMAT subroutine and first publication

To study the dynamic crushing response of parts made of composite material by Abaqus a FE model is developed. The FE progressive failure model of composite layers, including the damage initiations, damage evolution law, and element removal, is executed through a user-defined material subroutine (VUMAT) in ABAQUS/Explicit code. The FE model was validated by experimental test results obtained by the authors for cross-ply and angle-ply tubes subjected to axial impact and submitted the results as an academic paper to Composite Structure journal the status of the paper is presented in Figure 1.

The preparation of the paper has been started on 01/06/2020 and the paper was submitted on 22/04/2021.

The verified user-defined material subroutine will be used to investigate the lateral impact on the composite plate.



The screenshot shows the 'Submissions Needing Revision for Author pouria bahrami ataabadi' page. It includes instructions on how to download source files, submit revisions, or decline. Below the instructions is a table with one submission entry.

Action	Manuscript Number	Title	Initial Date Submitted	Date Revision Due	Status Date	Current Status	View Decision
View Submission File Inventory Revise Submission Decline to Revise Send E-mail	COMSTR-D-21-01470	Finite element modeling of crushing of CFRP cylindrical tubes under low-velocity axial impact	Apr 22, 2021	Aug 15, 2021	Jun 16, 2021	Revise	Revise

Figure 1. Publication status.

Since the paper is not revised yet, a draft version is presented in the following.

Finite element modeling of crushing of CFRP cylindrical tubes under low-velocity axial impact

P. B. Ataabadi^a, D. Karagiozova^b, M. Alves^a

^a Group of Solid Mechanics and Structural Impact, Department of Mechatronics and Mechanical Systems Engineering, University of Sao Paulo, Sao Paulo 05508900, Brazil

^b Institute of Mechanics, Bulgarian Academy of Sciences, Acad. G. Bonchev St., Block 4, Sofia 1113, Bulgaria

Abstract

The dynamic axial crushing response of cylindrical tubes made of unidirectional (UD) carbon fiber-epoxy material is investigated numerically with emphasis on generating realistic crushed modes and crushed morphologies. Two multi-layer models of laminated cylindrical tubes having different stacking sequences, namely cross-ply and angle-ply, were simulated using stacked layers of conventional 2D shell elements (S4R) bonded with the cohesive element interface model in ABAQUS. The FE progressive failure model of UD composite layers, including the damage initiations, damage evolution law, and element removal, is executed through a user-defined material subroutine (VUMAT) in ABAQUS/Explicit code. The so implemented progressive failure material model represented well the various crushing modes, including fragmentation mode, splaying mode, and axial splitting of UD lamina in the splaying crushing mode. The FE model was validated by experimental test results obtained by the authors for cross-ply and angle-ply tubes subjected to axial impact.

Keywords: Crashworthiness of composite tubes; Axial impact; Finite element modeling; User-defined material subroutine; Crushing mechanics.

1. Introduction

Composite materials like CFRPs, Carbon Fiber-Reinforced Plastics, are more expensive than conventional metals, however, their superior energy absorption per weight (SEA), has been proved to be beneficial in substituting heavy metallic absorbers with lighter composite ones, especially in the automotive and aerospace industries since weight is a critical design requirement. There are numerous extrinsic parameters, such as loading direction, environment effects, loading rate, and intrinsic parameters, like fiber volume fraction, fibers orientation, stacking sequence, that affect the crushing and energy absorption performance of composite absorbers. The various combinations of these parameters make the experimental development of the composite absorbers more costly than the current design of metallic ones. This highlights the importance of developing less expensive and reliable analysis tools to investigate the crashworthiness of composite materials.

The costs of the experimental procedure and limited application of existing analytical models ([1]) highlight the importance of developing reliable FE models capable of modeling complex crushing modes of composite materials subjected to dynamic

loading. Finite element analysis available in the commercial finite element packages such as LS-Dyna, ABAQUS, and PAM-CRASH are being widely used to predict the crushing behavior of composite structures under axial quasi-static and impact loading [2–7].

There is an ongoing huge effort to improve the reliability and accuracy of FE modeling of the axial crushing of tubular composite absorbers [4–6,8–10]. The main approach is modifying the existing 2D material models [11] or developing 3D constitutive models for the composite layers [5]. The force-displacement curve, SEA values, and crushing modes (crushed morphologies) have been considered to validate the numerical simulation when comparing with experimental results. In most of the above-mentioned publications, numerical models predict crashworthy criteria, like SEA and average crushing force, and force-displacement curves within reasonable accuracy.

Although there are several reports on similarities between crushed morphologies of experiments and numerical simulations, FE models have been less successful in reproducing the details of crushing modes of composite tubes under axial impact. For instance, to the best of the authors' knowledge, fragmentation mode and axial splitting of laminae in the splaying mode [12,13] have not been numerically well reproduced, even when using 3D elements and improved constitutive models [5].

Based on experimental works, it is evident that both intra-laminar (composite plies) and inter-laminar (delamination) damages affect the crushing behavior of these laminated tubes under axial impact. Therefore, FE multi-layer models, capable of modeling both intra-laminar and inter-laminar behavior, have been widely used to investigate the axial impact behavior of composite tubes in comparison to the FE single-layer models [14–16]. However, selecting the most appropriate finite element type, 2D or 3D continuum elements, to describe the thin composite plies is crucial. Since the composite laminae in a laminate tube under axial impact loading are likely to undergo significant bending deformation [12], the finite elements used to model these layers (intra-laminar model) should be capable of capturing bending behavior correctly [17].

The mid-surface shell elements (6 DOFs, three rotational and three translational DOFs at each node) could be excellent choices due to their reasonable bending behavior and computational efficiency. The plane stress (2D) shell elements with a mid-surface formulation in LS-Dyna have been widely used to simulate the stacked-shell composite parts under the axial impact [3,4,7,9,18–20]. However, conventional shell elements with the mid-surface formulation (S4R shell element) in ABAQUS have been rarely used (Zhu et al. [21], Zhao et al. [22]) to build multi-layer FE models of laminated tubes under axial

impact. This can be related to difficulties of bonding the two adjacent conventional shell layers with cohesive zone models in ABAQUS and poor out-of-plane behavior of conventional shell with the 2D formulation. In contrast to LS-Dyna, it seems that continuum elements, solid or thick continuum shell, are more popular finite element options to build up the laminated composite under axial impact by ABAQUS.

In theory, it is possible to incorporate 3D solid elements with one layer of bricks representing a ply of composite material. However, at least three to five solid elements through the thickness should be used to capture correctly the lamina bending response [23]. For example, Chiu et al. [4, 5] and Tan et al. [22, 23] have used three solid elements to represent the thickness (each lamina) in composite tubes and wedge under axial compression. Such models for relatively thin-walled and large-size structures are computationally inefficient since the continuum element thickness affects the stable time increment of the explicit solver [26]. Moreover, in theory, the technique of layering brick elements through the thickness of the relatively thin plate or shell components leads to an ill-conditioned set of equations [23]. It is important to note that the global response in terms of force-displacement characteristic, without a detailed stress analysis, does give sufficient information about the structural performance, as reported in most publications relevant to the axial impact on composite components in the literature.

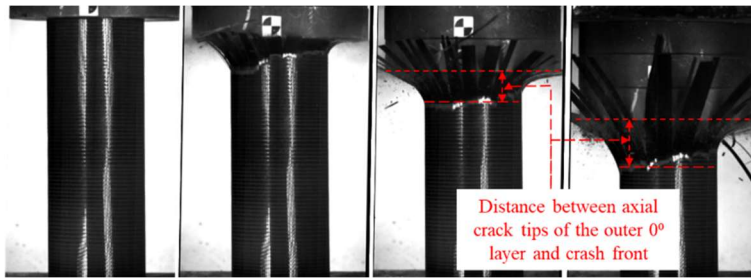
In ABAQUS Continuum shell elements (SC8R) rather than the conventional shell element (S4R) have been often used to model multi-layer laminated absorbers under an axial impact [11,27,28]. Although the continuum shell elements can be used for any thickness, thin continuum shell elements may result in a small stable time increment in FE Explicit solver, particularly for thin shell applications (like composite laminae) thus increasing significantly the number of increments taken to complete the analysis when compared to the same problem modeled with conventional shell element (S4R element) [26]. The continuum shell elements (SC8R) and conventional shell elements (S4R) have the same formulation in ABAQUS [26]. However, in contrast to the conventional shell (S4R), the continuum shell element discretizes the whole continuum body and has better contact behavior. Therefore, it is reported that models comprising a continuum shell have shown a more stable response under compressive loading than the S4R element [17]. This response characteristic can be related to the better contact behavior of the continuum elements related to interface modeling.

The present paper aims to investigate the performance of the conventional shell elements (S4R) in modeling the intra-ply (lamina) behavior of laminated tubes undergoing

axial impact, it has been less utilized in the literature. A user-defined material subroutine (VUMAT) will be used as a material model for the CFRP laminae. This material model is based on the MLT continuum damage mechanics (CDM) model and comprises many features of in-built progressive failure analysis (PFA) in ABAQUS, with a modified element deletion strategy to generate more realistic crushed morphologies. This modification will lead to the correct reproduction of the splaying, axial splitting, and fragmentation modes (ring-shaped debris) of UD laminae. The FE model was validated by experimental test results obtained by the authors [12].

2. Crushing response of laminated CFRP tubes under axial impact

Crushing response of laminated cylindrical cross-ply ($[0^\circ/(90^\circ)_2/0^\circ]_s$) and angle-ply ($[\pm 45^\circ/0^\circ/\pm 45^\circ/0^\circ/\pm 45^\circ/0^\circ/\pm 45^\circ]$) tubes made of unidirectional (UD) plies of CFRP, having 50 mm internal diameter and approximately 2.2 mm thickness, were investigated in Ref. [12] by using drop hammer test facility under different loading rates. Since the focus of the present work is on predicting the crushed modes in detail (crushed morphologies), a brief review of the crushing behavior of tubes and UD layers is present in the following. More details about the force-displacement curves and valuation parameters, like SEA and average crushing force, are presented in Ref. [12]. The bending behavior and crushed morphologies of the tubes and UD laminae during and after dynamic axial impact are presented in Fig. 1 and Fig.2.



(a)

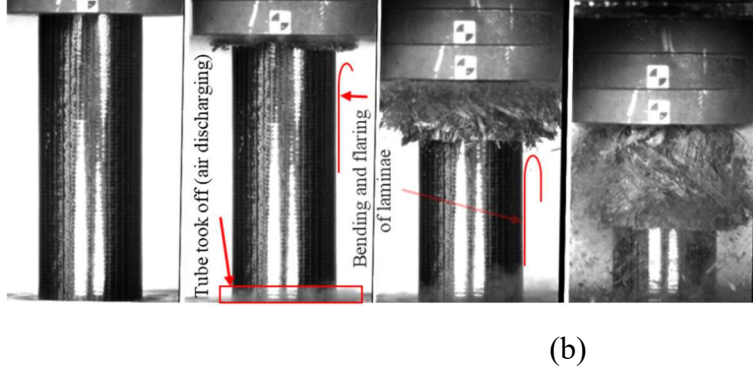


Fig. 1. Bending and damaging of the CFRP laminae under impact on laminated tubes; (a) Cross-ply tube ($[0/(90)_2/0]_s$), (b) Angle-ply tube ($[\pm 45/0/\pm 45/0/\pm 45/0/\pm 45]$).

When the laminate tubes are axially compressed, their laminae tend to undergo bending and separate from their surrounding layers. The bending behavior of each lamina is controlled by the hoop to axial (H: A) strength (stiffness) ratio of the lamina and its boundary condition imposed by the surrounding layers. For instance, the outermost 0° lamina in the cross-ply tube has low strength in the hoop direction and high strength in the axial direction, even the boundary being unrestricted on the outer side. This lamina starts to bend outwardly, and its diameter starts to increase. Thus, this layer undergoes tension in the hoop direction. The tensile stress in the weak resin-rich area in the hoop direction splits this layer into several long intact lamina bundles, splitting in splaying failure mode depicted in Fig. 2(a). A similar damage mechanism occurs for the innermost 0° layer of the cross-ply tube. The middle 0° layer is constrained at both sides of the surrounding 90° layers so that it splayed and split into shorter lamina bundles (brittle fracturing failure) than the outermost and innermost 0° layers Fig. 2(a).

The 90° layers experience bending but due to their low axial strength, these layers bent and broke into short length parts and formed ring-shaped debris. Such a fragmentation mode is shown in Fig. 2(a). The crushing modes observed in the cross-ply specimen in this study include all well-recognized crushing modes in a tube under axial compression; (I) Fragmentation mode, (II) Splaying mode, and (III) Brittle fracturing [29].

Fig. 3 presents the numerical replications of the above-mentioned crushing modes for UD laminae in a tube under axial impact generated by a FE model. This desired FE model has a robust intra-laminar progressive failure model with the capability of element deletion and of representing the main failure modes for a UD lamina like (I) tension

parallel to the fiber orientation, (II) compression parallel to the fiber direction, (III) tension transverse to the fiber orientation, (IV) compression transverse to the fiber direction.

However, even having a robust element deletion strategy in the intra-laminar model, the interface model affects the crushed appearances of composite laminae in the FE model. In other words, undamaged lamina bundles (splits) and ring-shaped debris and their combination (in Fig. 3) are controlled by both intra-laminar and inter-laminar models. The crushed morphology of the cross-ply tube consists of all characteristic crushed modes classified by Hull [30], includes splaying and tearing of laminae parallel to their fiber orientations, see Fig. 2(b), and it is more complicated than the crushed morphology of the angle-ply tube. Thus, a FE model that is capable of predicting the crushed modes similar to those observed in the cross-ply specimens under axial impact is more likely to reproduce the crushing performance of tubes having different stacking sequences like the angle-ply ones.

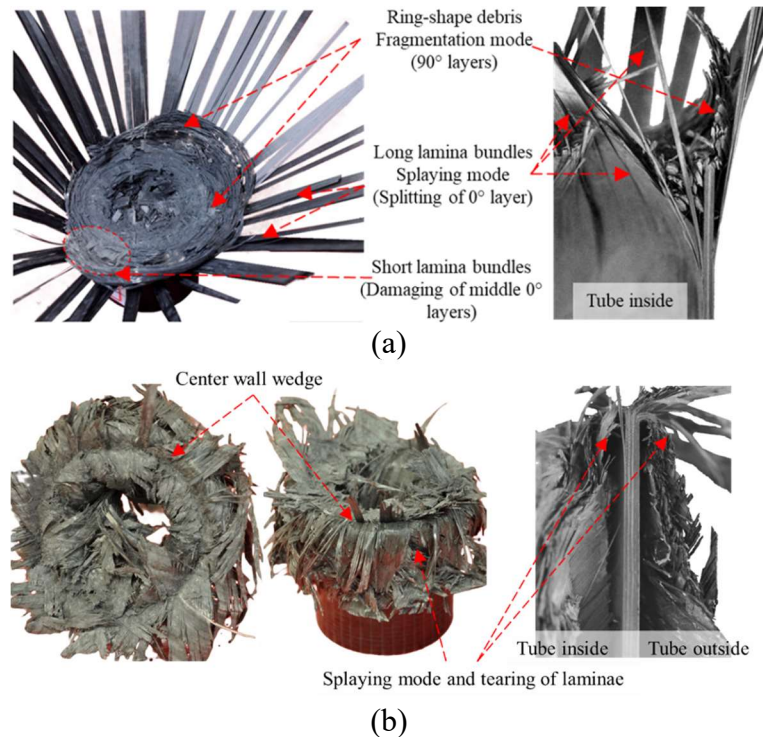


Fig. 2. Crushed morphology of CFRP tubes after axial impact; (a) Cross-ply tube [0°/(90°)₂/0°]ₛ; (b) Angle-ply tube [±45°/0°/±45°/0°/±45°/0°/±45°].

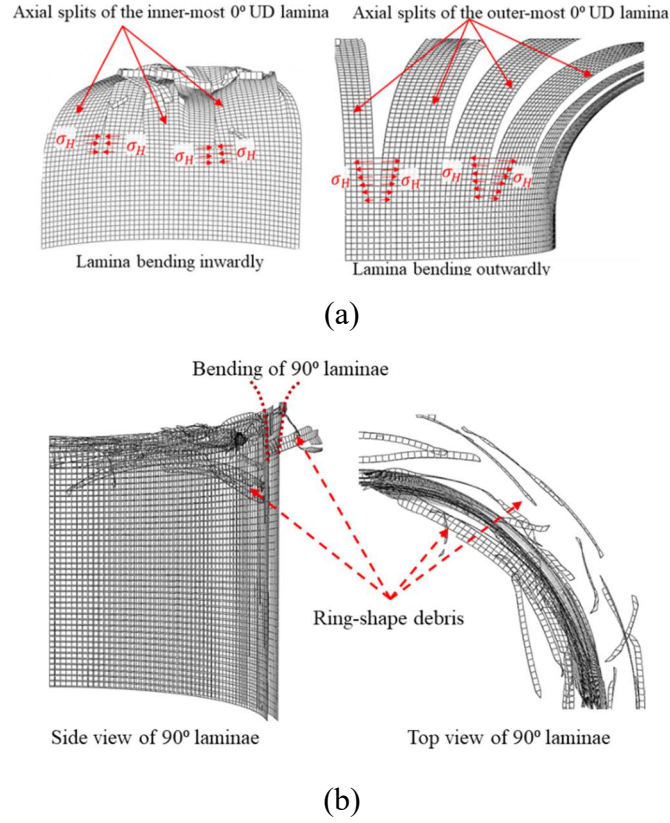


Fig. 3. Bending and damage mechanisms of splitting and splaying of 0° layers (a) and fragmentation of 90° layers (b).

Reports of successful numerical reproductions of axial splitting and ring-shaped debris in a laminated tube under axial impact loading are very rare in the literature. Palanivelu et al. [31] incorporated a few pre-defined axial seams in only some layers of a composite tube model, layers that are likely to fail and split in splaying mode, in order to increase the chance of generating the axial splits in the tube under axial impact. The axial splits in a cross-ply CFRP tube under axial compression have been reported by Chiu et al. [4, 5] who implemented a 3D finite element model in ABAQUS using an improved constitutive model for composite plies.

3. Description of the finite element model

Concentric layers of 2D shell elements (S4R in ABAQUS) were stacked to model the intra-laminar (composite plies) behavior of laminated tubes under axial impact loading. ABAQUS in-built cohesive element model was used to bond the adjacent composite laminae and simulate the delamination failure mode upon cohesive layers damage.

3.1 Intra-laminar failure modeling

ABAQUS offers a plane stress (2D stress state) progressive failure material model for fiber-reinforced plastic materials (FRPs) based on the MLT continuum damage mechanics (CDM) proposed by Matzenmiller et al. [32]. This material model uses Hashin's criteria that consider four different failure criteria for fiber and matrix under tension and compression. Recently, several 3D user-defined material subroutines (VUMAT) based on CDM have been published and incorporate some modifications, such as nonlinear shear behavior [5,33–35], modified element characteristic length [5] and load reversal [5,33,34]. Some of these material models were used to simulate the axial impact on the laminated tubes [5,6,11]. Although reasonable numerical (finite element) force-displacement (or SEA value) have been reported, the FE crushing modes do not share significant similarities with the experimental ones [5].

In the present study, it is assumed that the in-built plane stress Progressive Failure Analysis, PFA model in ABAQUS is sufficiently accurate to model the behavior of CFRP UD laminae in a tubular geometry under axial compression since the FE model can predict well the force-displacement curve. However, this model is not capable of generating realistic crushed modes (as those presented in Fig. 2) of composite tubes under axial impact. A simple study of pure tension (or compression) loading on a single S4R shell element can show that the in-built PFA model in ABAQUS for fiber-reinforced composites, by default, deletes the failed element only in the fiber direction. In other words, when loading (stress) is transverse to the fiber direction, the failed element will be only unloaded when the element deletion criterion is met, and this failed element will not be removed. This limitation can lead to the generation of unrealistic crushing modes of tubes made of UD laminae under axial impact.

3.1.1 Composite progressive failure material model

In the present paper, the user-defined material model (VUMAT) for the intra-laminar (composite plies) damage model is based on MLT continuum damage mechanics (CDM) for 2D stress state and shares many similarities with the constitutive material model in the PFA model of ABAQUS for FRP materials [26]. For composite UD layers four different failure modes; (I) fiber under tension, (II) fiber under compression, (III) matrix under tension, and (IV) matrix under compression, with a bilinear material response (Fig.4 (a)) for each failure mode will be considered. By introducing the

characteristic length, L^c that it is equal to the square root of S4R shell element size similar to the ABAQUS progressive failure model [26], the constitutive law is expressed as an equivalent stress-displacement relation ($\sigma_{eq} - \delta_{eq}$) instead of stress-strain relation to alleviate the mesh dependency during material softening. The equivalent displacement and stress for each of the four failure modes are presented in Appendix A.

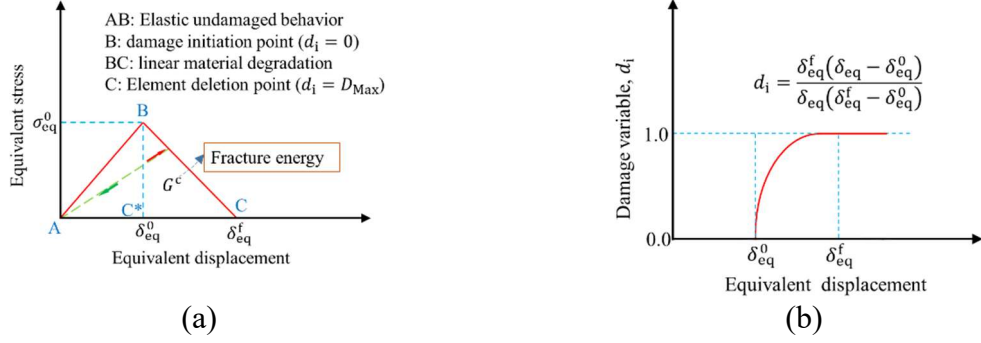


Fig. 4. The bilinear material behavior in the PFA material model in ABAQUS for FRPs and damage variable for a failure mode.

The response of the UD lamina will be expressed by Eq. (1), which represents the bilinear undamaged-damaged behavior of orthotropic material [26].

$$\sigma = C_d \varepsilon \quad (1)$$

where $\varepsilon = [\varepsilon_{11}, \varepsilon_{22}, \varepsilon_{12}]^T$ denotes the strain, $\sigma = [\sigma_{11}, \sigma_{22}, \sigma_{12}]^T$ is the true stress vectors, and C_d is the elasticity matrix of an orthotropic material in a 2D plane stress state. The elasticity matrix (\mathbf{C}) and its parameters can be written in the following forms [26].

$$C_d = \frac{1}{D} \begin{bmatrix} (1 - d_f)E_1 & (1 - d_m)(1 - d_f)E_1\nu_{21} & 0 \\ (1 - d_m)(1 - d_f)E_2\nu_{12} & (1 - d_m)E_2 & 0 \\ 0 & 0 & (1 - d_s)G_{12}D \end{bmatrix} \quad 2(a)$$

$$2(b)$$

where d_s , d_f , d_m represent the current state of damage in shear mode, the fiber direction (f), and transverse to the fiber direction (m), respectively. These three state variables should be calculated from four damage variables d_i^j in the 1- and 2-directions (1-direction is parallel to the fiber direction and 2-direction is transverse to the fiber direction) under compression or tension ($j = c, t$). The four damage variables ($d_f^t, d_f^c, d_m^t, d_m^c$) will evolve

from zero (at point 'B' Fig.4(a)) to one (at point 'C' Fig.4(a)) using a linear energy damage evolution law, as depicted in Fig. 4.

The Hashin's 2D failure criterion [36] is applied to predict the damage initiation (point 'B' in Fig. 4(a)) in mode I: Tensile stress parallel to the fiber direction ($\hat{\sigma}_{11} > 0$), Eq. (3), mode II: Compressive stress parallel to the fiber direction ($\hat{\sigma}_{11} \leq 0$), Eq. (4), mode III: Tensile stress transverse to the fiber direction ($\hat{\sigma}_{22} > 0$), Eq. (5) and mode IV: Compressive stress transverse to the fiber direction ($\hat{\sigma}_{22} \leq 0$), Eq. (6).

$$(3)$$

$$(4)$$

$$(5)$$

$$(6)$$

where $\hat{\sigma}_{11}, \hat{\sigma}_{22}, \hat{\sigma}_{12}$ are the components of the effective stress tensor, $\hat{\sigma} = \mathbf{M}\sigma$ used to evaluate the initiation criteria; σ is the true stress and \mathbf{M} is the damage operator.

$$(7)$$

with X^T, Y^T, X^C, Y^C being the strength parameters in tension and compression, respectively; S^L, S^T are the shear strengths parameter. It is assuming that the longitudinal and transverse shear strengths are equal.

In ABAQUS in-built progressive failure material model for composite materials, the shear damage variable (d_s) is a function of four in-plane damage variables ($d_s = f(d_f^t, d_f^c, d_m^t, d_m^c)$). However, in the present study the non-linear in-plane shear behavior the shear stress (τ_{12}) – shear strain (γ_{12}) relation in Eq. (8) was considered according to Donadon et al. [33,37] with an independent shear damage variable d_s . The non-linear in-plane shear behavior is presented in Fig. 5.

$$\tau_{12} = G(\gamma)_{12} \gamma_{12} \tag{8(a)}$$

$$G(\gamma)_{12} = G_{12} + c_1(e^{c_2 \gamma_{12}} - 1) \tag{8(b)}$$

where $G(\gamma)_{12}$ is the non-linear material model for in-plane shear modulus, G_{12} is the initial shear modulus, c_1 and c_2 are material parameters that will be calculated from the best fitting of in-plane shear tests.

A maximum strain criterion (Eq. (9)) is considered to compare the current shear strain (γ_{12}) to the maximum shear value (γ_{12}^0) to detect the shear damage onset.

$$\left(\frac{\gamma_{12}}{\gamma_{12}^0}\right)^2 \geq 1 \quad (9)$$

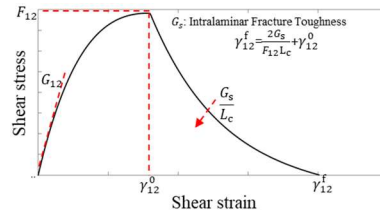


Fig. 5. Non-linear in-plane shear response.

The shear damage variable (d_s) will evolve by the Eq. (10) presented in Fig. 4(b) similar to the four other damage variables ($d_f^t, d_f^c, d_m^t, d_m^c$).

$$d_i = \frac{\delta_{eq}^f (\delta_{eq} - \delta_{eq}^0)}{\delta_{eq}^f (\delta_{eq}^f - \delta_{eq}^0)} \quad (10)$$

Besides the non-linear shear behavior, a major difference between the user-defined material subroutine (VUMAT) in the present work and the PFA material model in ABAQUS is related to the additional flexibility of the user-defined material model to control the element removal procedure by adding some features to the element deletion scheme of the material model.

3.1.2 Element deletion scheme

The progressive damaging material model for fiber-reinforced composite materials requires a robust element deletion scheme to avoid extremely distorted elements and to generate more realistic crush morphology, avoiding premature element deletion. Based on ABAQUS documentation [26], for all four above-mentioned failure modes, a failed element will be deleted when the damage variable (d_i) reaches the maximum damage

parameter specified by the user (point ‘C’ in Fig. 4(a)). However, element removal is an option. In other words, the material properties of the failed element will be degraded to zero (based on Eq. (2)) and the element will be removed at point ‘C’ corresponding to failure equivalent displacement (δ_{eq}^f) and $d_i = D_{Max}=1.0$. Hence, if the element deletion option was not activated by the user, the failed element only will be degraded but not removed from the simulation.

In the present work, the element deletion scheme of the above-mentioned material response (Fig. 4) was modified to allow more flexibility in the element deletion and avoid excessive element deformation for all four above-mentioned failure modes (tension and compression). Thus, a combination of damage variable parameter (first condition) and in-plane deformation gradient available in ABAQUS VUMAT as a tensor at each material point at the beginning of the increment (second condition) will be considered for each failure mode as follows.

Element deletion criterion

$$\{ \quad \quad \quad \} \quad (11)$$

When damage parameters $d_i^{T(C)}$ (i = fiber, matrix, T: Tensile, C: Compressive) reaches D_{Max} the corresponding component in the stiffness matrix will attain a small value (the condition I) and the failed element will be fully unloaded. However, the element will be deleted only if the second condition (deformation gradient) meets the specified values of $(F_i^{T(C)})$ selected by the user. In other words, the second condition causes a delay between element unloading and element removal. A trial-and-error procedure can be used to find proper values of $(F_i^{T(C)})$ corresponding to the second condition to avoid premature element removal, to control the damaging behavior of elements and to avoid excessive element distortion.

Fig. 5 describes the behavior of the above-mentioned element deletion strategy for a single shell element under uniaxial tension through comparing stress (σ), damage variable (d), and element statue (ES = 1: element active, ES = 0: element deleted from simulation). For the material model without considering the second condition (black dot lines), the failed element will be deleted (ES:1→0) when the damage variable reached the maximum specified value ($d_i = D_{\text{Max}}$). When considering both conditions (red lines), there

will be a delay between the element fully failure point (stress reached zero) and the element removal point. These two conditions make the FE model capable of a good prediction of the crush morphologies by adjusting $F_i^{T(C)}$ value.

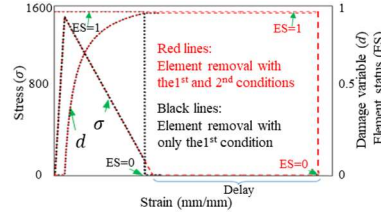
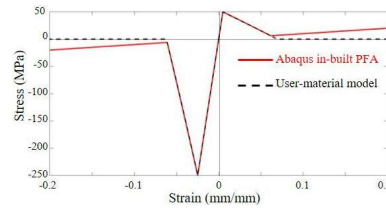


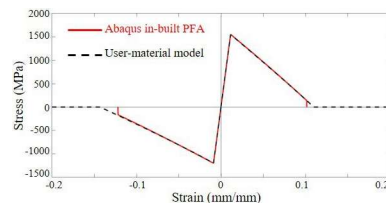
Fig. 5. The description of the element deletion strategy.

3.1.2 Performance of the modified user-defined material model (VUMAT)

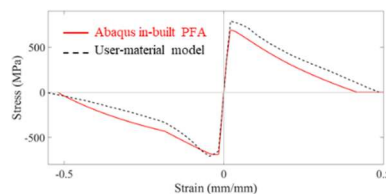
A material verification test for the user-defined material subroutine includes a set of single shell elements (S4R) subjected to tension/compression at some angles (off-axis angles) between the fiber direction and the loading direction. Fig. 6 presents the verification results for 0° , 45° , and 90° off-axis loading as solved by ABAQUS/Explicit solver. A reasonable correlation between stress-strain curves generated by the in-built PFA model and the modified user-defined material model implemented through the VUMAT subroutine is observed. The major difference is about element deletion control in Fig. 6(a); the failed element was not deleted in the in-built ABAQUS material model (red solid line in Fig. 6(a)).



(a)



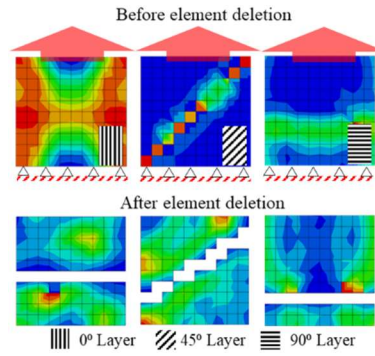
(b)



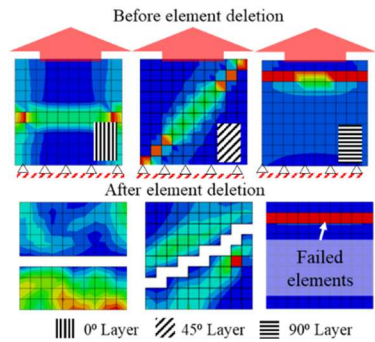
(c)

Fig. 6. Verification test of the modified user- defined material subroutine on an S4R element; (a) Fibers \perp loading direction; (b) Fibers \parallel loading direction; (c) 45° off-axis loading direction.

Fig. 7 compares the FE tensile simulation results of a coupon meshed with some 2D shell elements using the in-built progressive failure material model in ABAQUS and the modified user- defined material subroutine. The element deletion performance for three different angles (0° , $\pm 45^\circ$, 90°) between fiber direction and the loading direction compared between ABAQUS in-built progressive failure material model and the user-defined material. It is observed that when the loading direction is perpendicular to the fiber direction failed elements were not deleted in the ABAQUS in-built material model. However, the user-defined material model is capable of removing the failed elements in all three loading conditions.



(a)



(b)

Fig. 7. Element deletion performance of progressive failure model; (a) The user-defined material model (VUMAT); (b) ABAQUS in-built material model.

3.2 Inter-laminar (interface) model

Since the interface thickness in laminated composites is negligible, the tie-break in LS-Dyna and surface-based cohesive model (CZS) in ABAQUS are the ideal techniques

to bond the adjacent laminae. Tie-break interaction has been predominantly utilized to bond the mid-surface shell elements in LS-Dyna to model multi-layer composite tubular absorbers under axial impact [3,4,7,9,18–20]. However, very few successful multi-layer models using CZS and conventional shell elements (S4R) have been built when using ABAQUS [38] for composite tubes under axial impact. In contrast, the CZS bonding method has been used to tie adjacent layers of continuum elements, continuum shell, and solid elements, to simulate the axial impact on tubular composite components [6,11,39,40] in ABAQUS. Although simulations that used the S4R element together with the CZS in ABAQUS have been seldom reported for tubular composite structures undergoing axial impact, some researchers (Zhu et al. [21], Zhao et al. [22]) have tied the S4R elements when using element-based cohesive zone model (CZE) in ABAQUS to model laminated tubes under axial impact. The CZE technique adds extra continuum elements to the FE model and their small thickness affects the stable time increment thus increasing significantly the computational cost [41]. However, the combination of S4R-shell layers of composite bonded together with CZE still has computational advantages against the models built of continuum layers of composite bonded with the CZS method.

Although energy dissipated due to damaging of a weak resin-rich interface is negligible in comparison to the dissipated energy by composite laminae, an incorrect FE model of the interface may result in poor simulation results of composite tubes under axial impact. In other words, underestimating/overestimating of mechanical properties of the interface could lead to too low (or too high) crushing force and wrong crushing modes (morphologies). In the present work, the in-built cohesive element technique will be used to model interface layers. Cohesive zone element (CZE) with a bilinear response based on traction-separation law has been considered. The maximum stress criterion and a linear energy degradation law were selected to model damage initiation and post-damage behavior of the interface layers, with the details being presented in Appendix B.

4. Description of the FE model of axial impact on tubes

A quarter model of tubes ($\frac{1}{4}$ model with symmetry boundary conditions with respect to the displacement and rotational degrees of freedom (B.C1 and B.C2)) was considered for both cross-ply and angle-ply tubes to speed up the simulation process [5], as presented in Fig. 8. It was found from the drop test results [12] that the chamfer angle has no significant effect on the crashworthy parameters like average crushing force and SEA of tubes under impact so that only 45° external chamfer with stepped-wall geometry has been

modeled numerically in the present study. Details of the 45° external chamfer used as a crush trigger are shown in Fig. 8. The main parameters of the tubes are given in Table 2. Tubes are placed on the fixed rigid plate freely. The general contact interaction with tangential behavior (friction coefficient equals 0.3) and normal behavior (hard contact) interactions have been applied between all surfaces in the models. It was reported in Ref. [12] that the crushing performance of CFRP cylindrical tubes in the present study is not strain rate sensitive. Thus a rigid impactor having only vertical transitional movement, with 102 kg mass and 7 m/s initial velocity will impact the composite tubes instead of considering all impact conditions in Ref. [12]. The diameter of the impactor in FE models equals the physical impactor in the experiments. This dimension is important since the outermost 0° lamina bundles escaped from the impactor in the cross-ply specimens. The work done by gravity was included in the model.

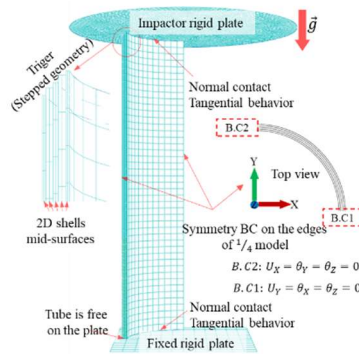


Fig. 8. FE model of 1/4 tube.

Basic mechanical properties of unidirectional CFRP prepreg material in this study, e.g. elastic moduli, shear modulus, Poisson's ratio, and strengths, were back-calculated from testing of specimens cut from the composite cross-ply and angle-ply tubes [42] and are listed in Table 1.

Table 1. Mechanical properties of unidirectional carbon fiber epoxy material.

Property	Symbo l	Units	UD prepreg
Density	ρ	Kg/m ³	1600
Elastic modulus 0°	E_1	GPa	136.32
Elastic modulus 90°	E_2	GPa	9.30
In-plane shear modulus	G_{12}	GPa	5.10
Major Poisson's ratio	ν_{12}	-	0.294
Ultimate tensile strength 0°	X^T	MPa	1550
Ultimate tensile strength 90°	Y^T	MPa	1200*
Ultimate compressive strength 0°	X^C	MPa	50*

Ultimate compressive strength 90°	Y^C	MPa	250*
Shear Strength	$S (F_{12})$	MPa	74.00
Tensile fracture energy, fiber direction	G_f^T	N/mm	91 [6]
Compressive fracture energy, fiber direction	G_f^C	N/mm	79.9 [6]
Tensile fracture energy, transverse to fiber	G_m^T	N/mm	1.35**
Compressive fracture energy, transverse to fiber	G_m^C	N/mm	4.2**
Parameters of nonlinear shear behavior (Eq.(8))	C_1	-	4.85e3 [†]
	C_2	-	-29.95 [†]

* Provided by the tubes' manufacturer.

** Values are calculated by using Eq. A.1 to A.4 for an S4 shell element with unit dimension.

[†] C_1 and C_2 are calculated from curve fitting of shear stress-strain data presented in Ref. [42].

Fracture toughness energies of composite plies (G_f^T , G_f^C , G_m^T , G_m^C) have significant effects on both force-displacement curve and crushing modes of CFRP tubes under axial impact. Compact Tension (CT) and Compact Compression (CC) tests have been used by several researchers [22,43] to determine fiber-dominant fracture energies (G_f^T , G_f^C) of the composite material to find intra-laminar fracture energies in order to simulate the axial crushing of composite absorbers. The data input for matrix-dominant fracture toughness energies (G_m^T , G_m^C) in several studies [6,8] are considered to be equal to the inter-laminar (interface) fracture energies. However, the majority of studies of the axial impact on laminated tubes adopted the fracture energies available in the literature.

To the best of the authors' knowledge, there are no available fracture energies for the CFRP material in the present study. Moreover, adopting the fracture energies, especially matrix-dominant (G_m^T , G_m^C), from the literature was problematic in the current model. To avoid numerical issues like snap-back, for all failure modes the input value of fracture toughness energies for a FE element should be greater than elastic energies (energies absorbed by element up to failure onset). If input values for fracture energy in a particular failure mode are lower than the elastic energy, ABAQUS ignores the input value. Thus, the failed FEs will be instantaneously unloaded when damage initiation is met, i.e., the elements will not experience a progressive and gradual material degradation after damage initiation onset point 'B' in Fig. 4(a). Instantaneous unloading of failed elements leads to poor stress redistribution between the failed elements and their neighbor FE elements and eventually leads to a low global bearing-load of the laminated structure. For a particular failure mode, the elastic energy is a function of element characteristic length (L_C), elastic parameters, and strength of composite ply. These minimum values can be calculated from Eq. (A.1) to (A.4) based on the ABAQUS user's manual. The effect

of selecting different values of matrix compressive fracture toughness energy (G_m^C) on the response of a single S4R shell element (1.0×1.0 mm size) under compressive load transverse to the fiber direction is illustrated in Fig. 9.

In most of the publications related to ABAQUS numerical simulation of axial impact on laminated absorbers, the fiber-dominant fracture energies are approximately 9 times the elastic energy (if considering an element with unit mesh size). However, the matrix-dominant fracture energies are even less than elastic energy for a unity element. Thus, the mesh size should be selected by considering the matrix-dominant fracture energies to avoid the above-mentioned problem. Very fine mesh size is required, for instance, a size of 0.25 mm × 0.25 mm was adopted in Ref. [8], which is computationally inefficient for a multi-layer FE model of relatively large laminated components. Therefore, in the present work the matrix-dominant toughness energies, G_m^T, G_m^C , are calculated by Eq. (A.1) to (A.4) for an S4R shell element with the unit area instead of refining the mesh size. Since the mesh sizes in the present study are smaller than 1 mm, the failed finite elements will undergo a gradual progressive uploading process. This modification on the matrix-dominant fracture energies is vital to generate realistic crushing modes. This modification also may slightly increase the predicted load-bearing capacity of the tubes.

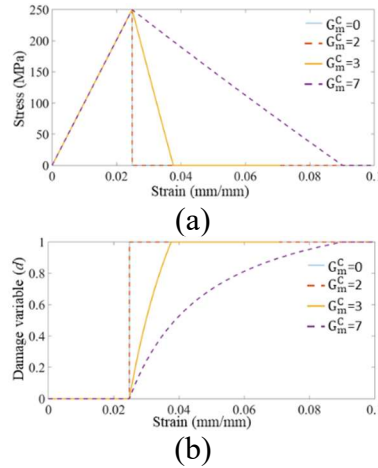


Fig. 9. Effect of matrix compressive fracture toughness energy (G_m^C) on a single element behavior under compression transverse to the fiber direction; (a) Stress-strain curve; (b) Damage variable-strain curve.

Table 2. Tube geometry [12].

Item	Angle-ply specimen	Cross-ply specimen
Stacking sequence ^{1,2}	$[\pm 45/0/\pm 45/0/\pm 45/0/\pm 45]$	$[0/(90)_2/0]_s$
Inner diameter (mm)	50.00	50.00
Outer diameter (mm)	54.70	54.38
Mass per length (g/mm)	0.59	0.54

¹ 0° , $\pm 45^\circ$, and 90° are measured from the tube axis.

² **Bold layers** are 300 gsm Unidirectional (0.3 mm thick) and the others are 200 gsm Unidirectional (0.2 mm thick).

The parameters $F_f^{T(C)}$ $F_m^{T(C)}$ for element deletion in the fiber and transverse to the fiber directions were selected through a trial and error procedure by simulating the axial impact on the cross-ply tube to generate desired crushing modes presented in Fig. 2(a). The effect of these parameters ($F_f^{T(C)}$ and $F_m^{T(C)}$) is presented in Fig. 10 comparing simulation of axial impact on the cross-ply tube. The material model with the higher values of $F_f^{T(C)}$ and $F_m^{T(C)}$ reproduce better the features of crushed modes of the cross-ply specimens under axial impact.

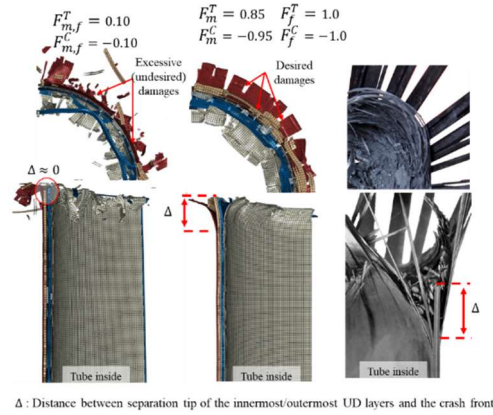


Fig. 10. Effect of selecting the different values for $F_i^{T(C)}$ on element deletion.

The mechanical properties of interface layers were adopted from the literature, as listed in Table 3. The elastic parameters, E_n , E_t , E_s were obtained from Ref. [8], the peak strengths, t_n , t_t , t_s and fracture toughness values, G_I , G_{II} , G_{III} of the interface layers were obtained from Ref. [6]. Some preliminary simulations of axial impact on the cross-ply tube using initial mechanical properties of the interface layer (listed in Table 3) showed uncontrolled and undesired separation (large delamination) between the outermost layer and their adjacent layers. This fast separation may lead to a low average crushing force

on the tube in comparison to the experimental impact tests. Some of these values were adjusted through a trial-and-error simulating of axial impact on the cross-ply specimen to increase the average crushing force on the tubes in this study. The initial and adjusted mechanical properties of cohesive layers are listed in Table 3.

Table 3. Mechanical properties of interface layers.

	Symbol	Initial values	Adjusted values
Elastic parameters [8]	E_n	2.970	2.970
	E_s	1.080	1.080
	E_t	1.080	1.080
Critical fracture toughness (N/mm)	G_I	0.55 [6]	0.55*
	G_{II}	1.55 [6]	1.55
	G_{III}	1.55 [6]	1.55
Peak strength (MPa)	t_n	54 [6]	57.8*
	t_s	70 [6]	70
	t_t	70 [6]	70

* Adjusted values with simulating of axial impact on the cross-ply specimen.

Note: The cohesive property parameter $\eta = 1.45$ is selected.

Layers of 8-node three-dimensional cohesive elements (COH3D8) with 20- μm thickness have been inserted between the adjacent concentric composite layers. The surrounding composite laminae are bonded to the cohesive layers with rigid tie interaction (surface-to-surface formulation). Figure 11 illustrates the connectivity of layers in the stacked-shell models of the present study.

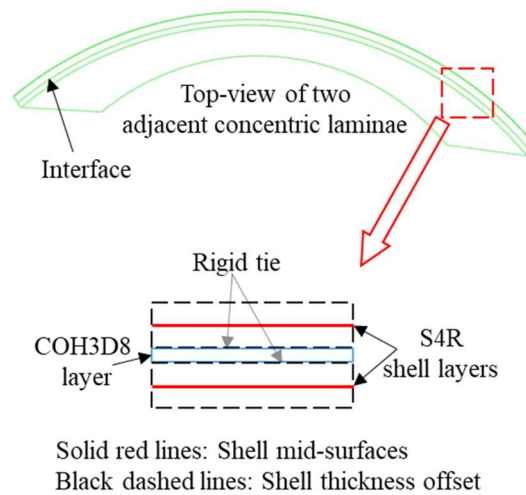


Fig. 11. Layer connectivity in the stacked-shell models in the present study.

5. Results and discussion

5.1 Results for the cross-ply specimen

The finite element model of the cross-ply tube consists of five layers of the S4R shell element. The outermost and innermost layers are discretized by 0.7×0.7 mm element and the other layers are meshed with 0.60 mm mesh size. Figs. 12-13 show the FE crushed modes and force-displacement curve of the axial impact simulation of the cross-ply tubes using initial mechanical properties of the cohesive layers. Figure 12 shows that the FE model had predicted the main characteristic features, including long lamina bundles of the outermost and innermost 0° UD layers and ring-shaped debris of 90° UD layers. However, the ring-shaped debris in the experimental tests remained more intact in contrast to the ring-shaped debris in the FE model, which split into several shorter segments.

Figure 13 compares the predicted crushing force by the FE model with the experimental results. The average crushing force of the numerical model is about 7kN (24 %) lower than the average crushing force obtained during experimental tests. Part of this difference is due to the simulation of the FE $\frac{1}{4}$ model, which does not retain full symmetry upon damage development. Note that the present FE model does not take into account the full effect of debris interaction inside the tubes as well as the possible effect of trapped air inside the tubes during crushing on the energy dissipation and crushing force. In the present study (likewise the literature) the delamination has been considered to occur inter-laminarly, however, the post-impact investigation in Ref. [12] shows that separation of the outermost layer occurred as an intra-laminar failure.

The outermost 0° layer separated from the adjacent layer faster away from the crush front (Fig. 12); consequently, a negligible amount of impact energy has been dissipated through this damaging mechanism. Therefore, adjusted values for mechanical properties of interface layers have been used to restrict the unstable delamination of the outermost layer in the following. This measure may increase the dissipated energy and eventually increase the average crushing force. Although, an increase in mechanical properties for composite layers, like fiber-dominant, may alleviate the low crushing force significantly. This measure was not considered in the present study.

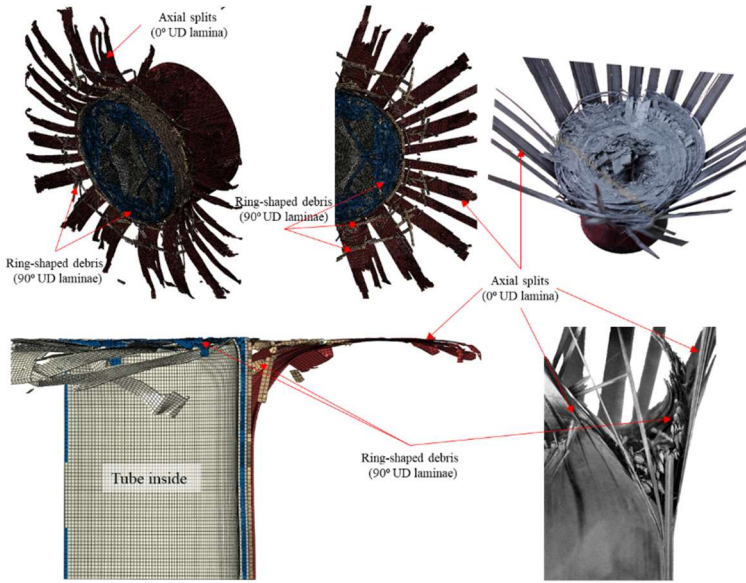


Fig. 12. The crushing modes of the cross-ply tube under axial impact with the initial input values for cohesive layers.

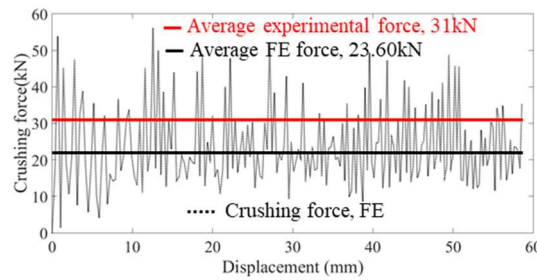


Fig.13. Force-displacement curve for cross-ply tube under axial impact with initial input values for cohesive layers.

Numerical results for axial impact on the cross-ply specimen with adjusted cohesive mechanical properties are presented in Fig. 14 and 15. This modification led to a higher crushing force (1.8 kN increased), however, the average crushing force remains 18% (5.6kN) lower than the average crushing force observed in the experimental study [12]. The new stronger interface layers kept the composite more tightly together with more restricted separation. Thus, composite laminae experienced more intense damage, and eventually, more impact energy was dissipated. For instance, the axial splits of the outermost/innermost 0° UD composite layers have experienced more damages (broken in shorter splits) in the FE model with adjusted cohesive mechanical parameters, Fig. 15. However, there are many similarities between crushed morphologies of the experimental and numerical cross-ply tube under axial impact. The major difference between the results of the model with initial cohesive parameters and calibrated one is obvious when

comparing the propagation of delamination in the outermost/innermost 0° UD layers in Fig. 12 and Fig. 15.

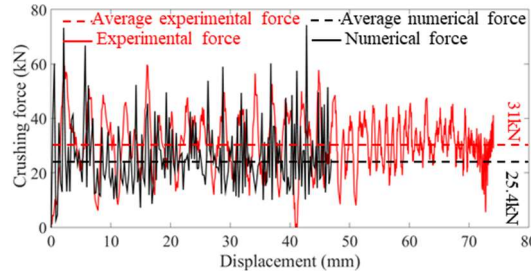


Fig. 14. Force-displacement curve for cross-ply tube under axial impact with calibrated input values for cohesive layers.

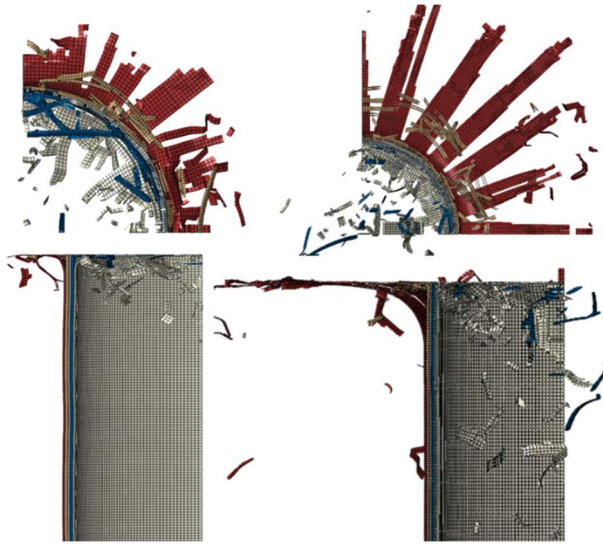


Fig. 15. The crushing modes of the cross-ply tube under axial impact with calibrated input values for cohesive layers.

4.2 Result for crushing of the angle-ply specimen: FE model transferability

In order to evaluate the validity and transferability of the FE model, the angle-ply tube $[\pm 45/0/\pm 45/0/\pm 45/0/\pm 45]$, was simulated by using the material subroutine and the above-mentioned material properties. Each pair of ± 45 layers considered and modeled as a single equivalent layer. All layers in this model were meshed by S4R elements with 0.6×0.6 mm. The bending and crushing behavior of the angle-ply tube are presented in Fig. 16. The FE model reproduced the bending behavior of composite laminae correctly,

leading to a similar global crushed appearance in comparison to experimental crushed morphologies. The 0° UD laminae (fibers parallel to the tube axis) were split axially, however, the $\pm 45^\circ$ layers bent correctly but remained almost intact, and the tearing of these $\pm 45^\circ$ layers, observed in the post-impact investigations, was not well predicted by the FE model.

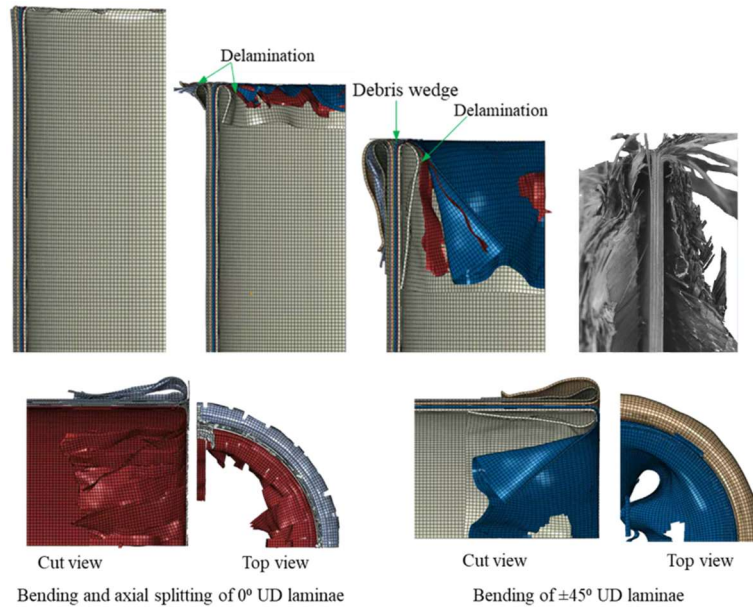


Fig. 16. Bending and crushing behavior of the angle-ply tube under the axial impact.

The crushing forces of FE simulation and experimental test on the angle-ply specimen were compared in Fig. 17. The average crushing force of FE simulation is about 11% lower than the average crushing force on the angle-ply in the experimental tests. This difference is caused by the simulation of the $\frac{1}{4}$ model of the tube, which can not fully account for the interactions (friction and compaction) between trapped debris inside the tube and possibly by the effect of air trapped inside the tube during compression, which was not considered in the present study.

Figures 14 and 17 illustrate that the magnitudes of oscillations of cross-ply and angle-ply were generated correctly by using the finite element model. The force profile of the cross-ply specimens under dynamic impact was characterized by a larger oscillating magnitude when compared to the angle-ply specimens. There is an agreement between FE simulations and experimental observations on this issue.

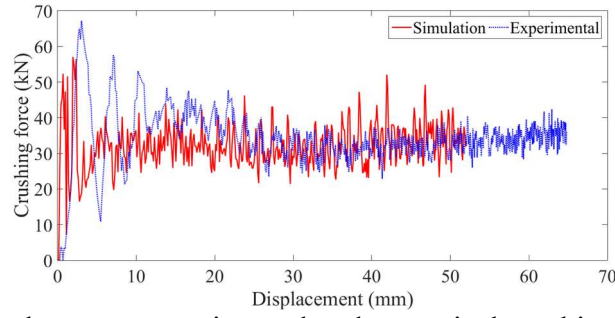


Fig. 17. Comparison between experimental and numerical crushing forces of the angle-ply specimen under the axial impact.

5 Conclusions

Crushing performance of composite tubes under axial impact was predicted by using a computationally efficient FE model consisting of 2D shell elements (S4R shell element with mid-surface formulation) and cohesive element interface layers in ABAQUS/Explicit. The present study shows the benefits of conventional shell elements in ABAQUS to model axial impact on laminate absorbers which has been less considered in the literature.

Intra-laminar model of unidirectional FRP was submitted to the ABAQUS/Explicit solver via a user-defined material subroutine (VUMAT) that shares many similarities with the ABAQUS progressive failure model with the modified element deletion strategy. The modified element removal scheme enabled the FE model to reproduce some of the well-recognized crushing modes of composite laminae under axial impact loading, e.g. axial splitting-splaying mode, and ring-shaped debris (fragmentation mode). Besides the generation of realistic crushing modes, a reasonable correlation between the valuation criteria generated with the FE model and experimental results was observed.

Finite element models of laminated tubes under axial impact loading, capable of generating fragmentation mode (ring-shaped debris in UD laminae having fiber in the hoop direction of the cross-ply tube) were so far not reported in the literature as it was here done. Replication of axial splitting in the splaying mode in the present simulation work is also rarely reported in the literature. In some publications, pre-defined axial seams in the few layers of a model, likely to fail in splitting mode, are used to model axial splitting [31]. However, in the present study, all layers are modeled in the same manner without any special consideration.

Acknowledgments

The financial support from Brazilian funding agency FUSP for this research is gratefully acknowledged.

A second paper with the same topic of the above-present manuscript is under preparation to be submitted soon.

Part II: Experimental and other activities at GMSIE laboratory

The main objective of the present project is to investigate the lateral impact on the metallic and composite plates as the main part of obtaining the fuel tank safety certification by the client (Embraer). The report about activities related to this part (launching a cubical projectile, designing a new gas-gun facility to launch projectiles at 250 m/s velocities, designing SABOTS, and preparation high-speed cameras and other required sensors) was delivered for a period of 01/06/2020 to 31/12/2020. Due to abnormal conditions due to the covid 19 pandemic and the problem of Embraer to finalize the dimension of specimens and other testing conditions this part of the project is paused. The GMSIE laboratory is waiting to receive the specimens and cubic projectiles to continue the project (September 2021 is the prevision date of providing the specimens). However, other laboratory activities are allocated to the candidate to keep the project active. These activities include the experimental numerical study of the impact safety of motorcycle helmets in the Brazilian market (the helmet safety project is funded by FAPESP).

Part 2: Activities related to the helmet safety project

The flow diagram for the helmet safety project is presented in Figure 2.

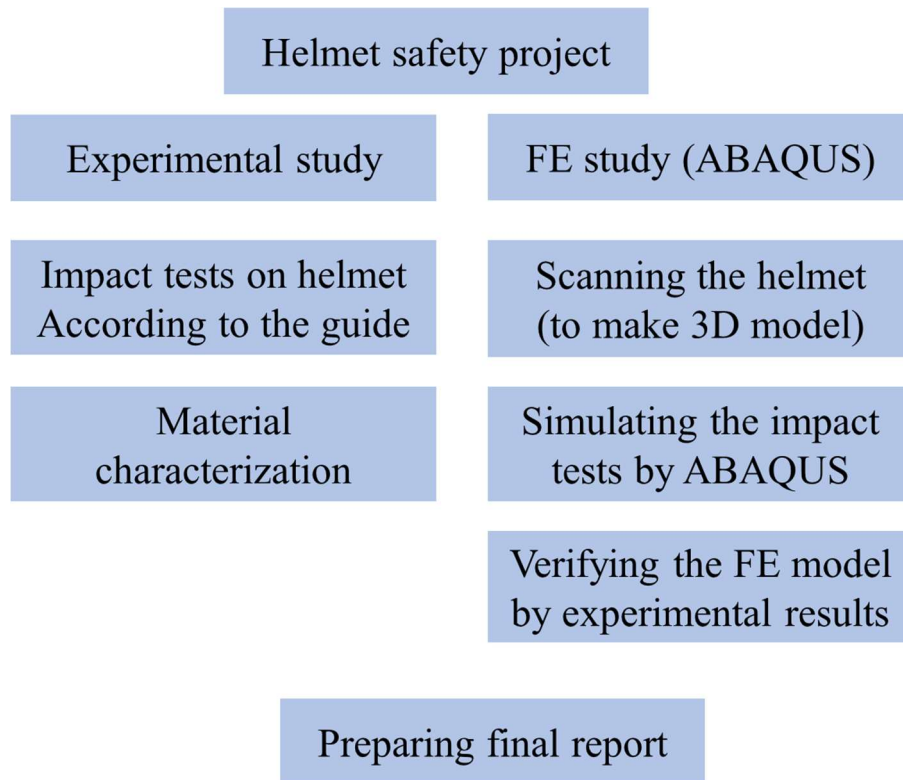
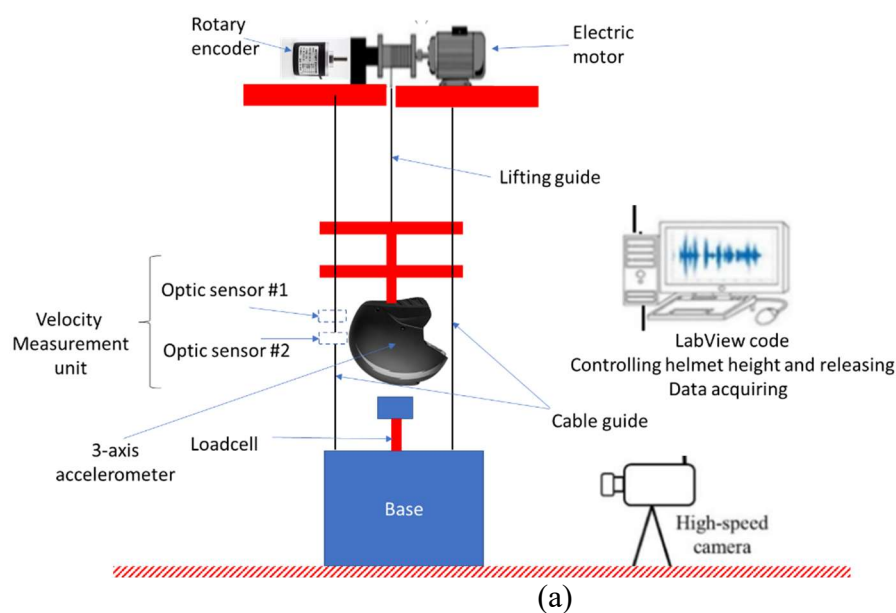


Figure 2. Helmet impact safety study.

Experimental study of helmet safety

The set-up and some of the equipment are presented in Figure 2. The helmet rig was available in the GMSIE laboratory; however, new modifications are applied to the set-up by the candidate.



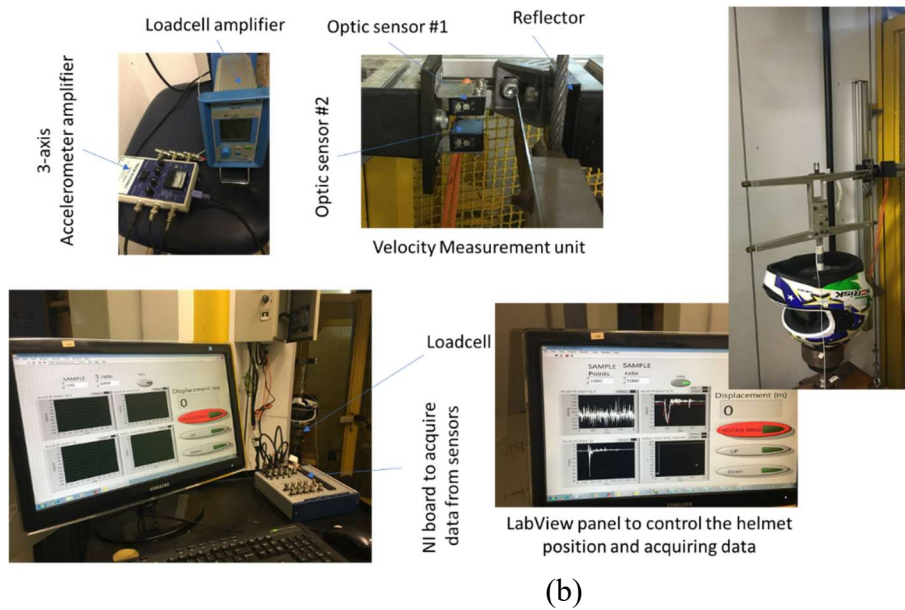


Figure 3. helmet test set-up; (s) schematic overview of the rig at GMSIE laboratory and (b) equipment.

- Modifications to the helmet rig at GMSIE laboratory
 - Installing a Rotary encoder to measure the height of the helmet from the base automatically and more accurately.
 - Developing a new LabVIEW code to control the helmet position, starting the test, and acquiring the data from sensors.
 - Installing a 3-axis accelerometer to study the rotational acceleration of headform.
 - Installing load-cell to measure the force on the helmet.
 - Using optic sensors and reflectors to measure the velocity of the helmet just before impact.

Set-up is completed and preliminary tests are undergoing to check the accuracy and repeatability of equipment during tests.

The experimental setup will be used to investigate the safety of helmets in the Brazilian market and used to verify the virtual testing tools (FE modeling). An example of the acceleration-time history of the impact test is presented in Figure 4.

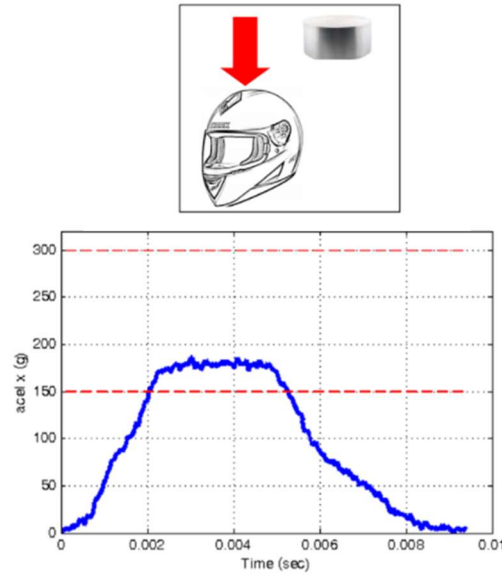
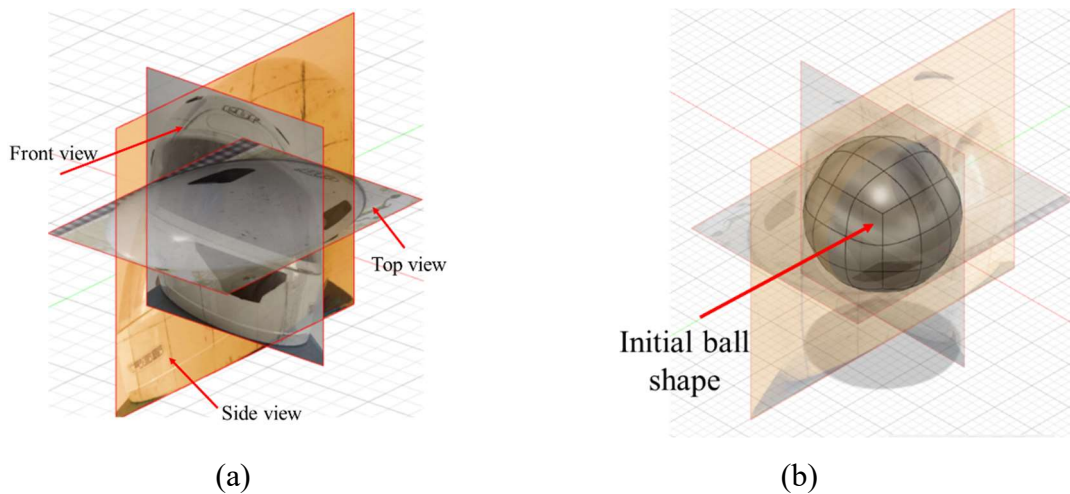


Figure 4. Example of the acceleration time history of impact test on the helmet during preliminary tests.

Numerical (FE) study of helmet safety

To simulate the impact test on the helmet, first, it is necessary to generate a 3D model of the helmet. In the beginning, 3 perpendicular photos from the helmet and inner foam were taken then by using Fusion 360 a 3D model of the helmet was generated. Figures 5-7 show the procedure for this model generation. However, this method was time-consuming and was not fully accurate. Thus, another method based on photogrammetry was developed for the generated virtual model of the helmet.



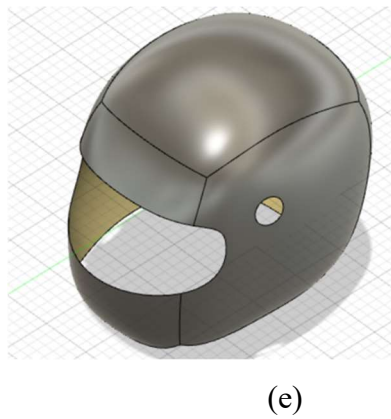
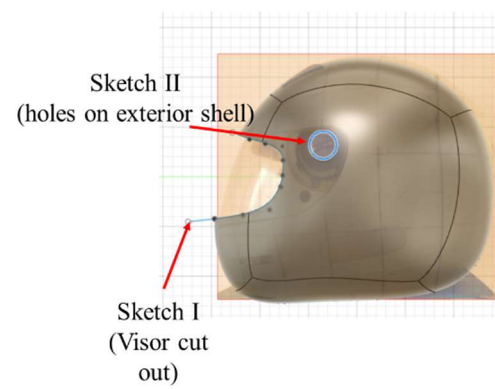
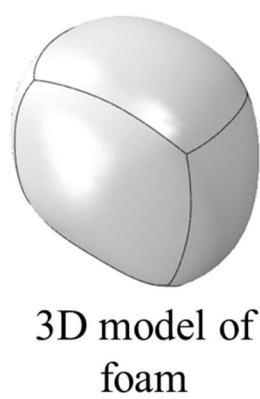


Figure 5. The procedure of generating the 3D model of the helmet; (a) Three perpendicular canvas, (b) initial 3d ball form, (c) rough 3d model of helmet, (d) Sketches on the 2D canvas, (e) Three-dimensional model of helmet exterior surface, (f) FE model of the exterior shell.



(a)



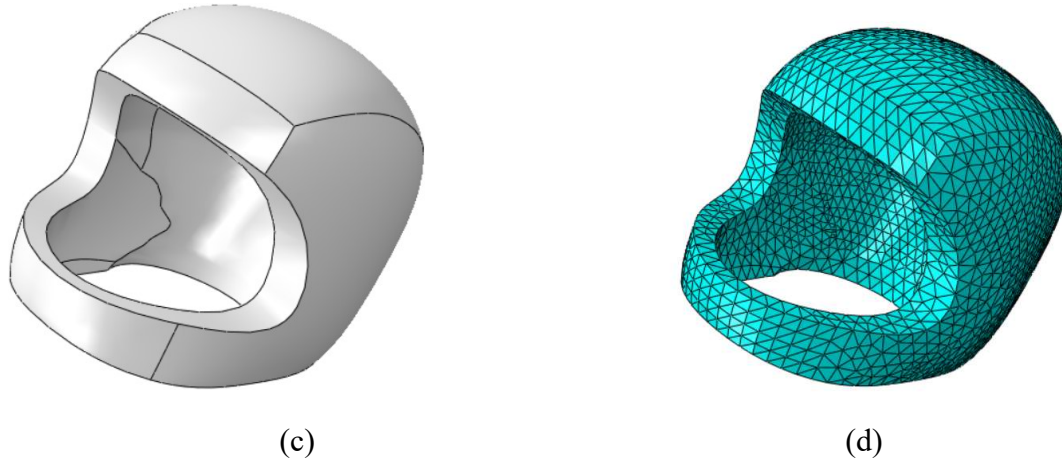


Figure 6. Protective foam model: (a) Rough 3D model imported into ABAQUS; (b) Head form used for modifying foam part, (c) 3D model of the protective foam, (d) FE model of protective foam.

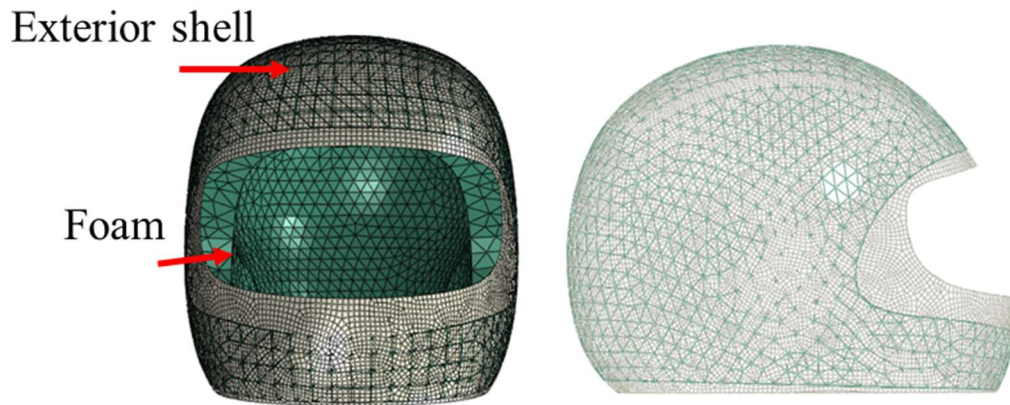


Figure 7. FE assembled a model of the helmet in ABAQUS.

A virtual model of the helmet by photogrammetry technique

Photogrammetry is the technology of obtaining reliable information about physical objects through the process of capturing, measuring, and interpreting images, see Figure 8.



Figure 8. Photogrammetry.

Following activities have been done to make the virtual models of the helmet by using photogrammetry.

- Making set-up to capture images from different angles and positions from the object; including a rotating base (presented in Figure 9).
- Learning and using the *Agisoft Metashape* program to generate 3D virtual models from captured images (see Figure 10-11).
- Learning and using software to edit virtual models; like *Fusion 360* and *blender software*.

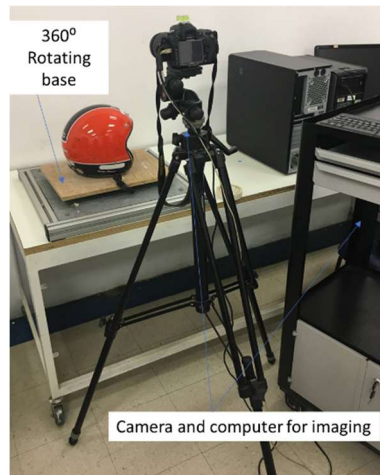
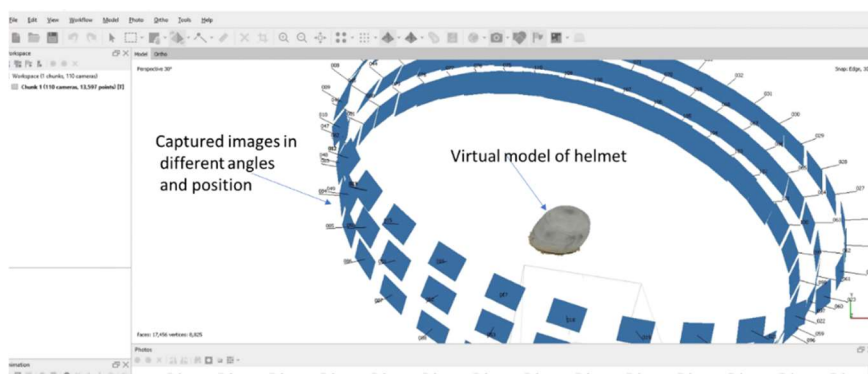
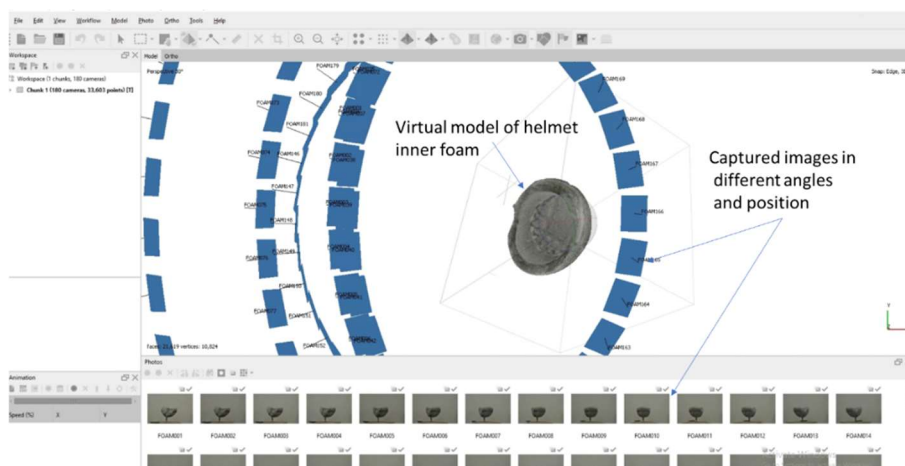


Figure 9. Setup to capture images.



(a)



(b)

Figure 10. Virtual 3D model of the helmet; (a) external shell of the helmet, (b) foam inside the helmet.

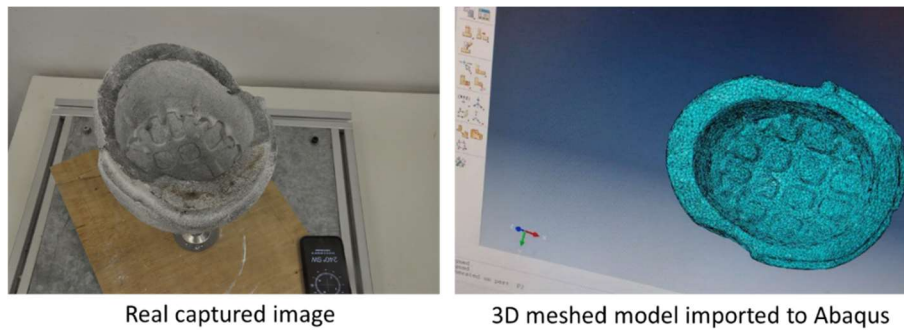


Figure 11. Comparison between the real captured image and generated 3D model.

The 3D model of the helmet with high accuracy and small details will be imported to the ABAQUS to simulate the impact tests with different scenarios. After validating the FE model with experimental tests, for other helmets available in the Brazilian market only numerical assessment will be used to check the safety of these helmets. This procedure will decrease the cost of helmet safety assessment.

Part III: other activities

- Making tutorial for the class PMR5026 - Elementos Finitos Linear: Teoria, Programação e Experimento).
- Teaching Abaqus one session (2 and half hours).
- Preparation for material characterization tests of polymeric material for making railroad sleepers.
- Preparation and writing the second article.